GPU Based Real-time Instrument Tracking with Three Dimensional Ultrasound

Paul M. Novotny[1], Jeffrey A. Stoll[2], Nikolay V. Vasilyev[3], Pedro J. Del Nido[3], Pierre E. Dupont[2], and Robert D. Howe[1]

[1] Division of Engineering and Applied Sciences, Harvard University, MA USA
[2] Department of Aerospace and Mechanical Engineering, Boston University, MA USA
[3] Department of Cardiovascular Surgery, Children's Hospital Boston, MA USA

Abstract. Real-time 3D ultrasound can enable new image-guided surgical procedures, but high data rates prohibit the use of traditional tracking techniques. We present a new method based on the modified Radon transform that identifies the axis of instrument shafts as bright patterns in planar projections. Instrument rotation and tip location are then determined using fiducial markers. These techniques are amenable to rapid execution on the current generation of personal computer graphics processor units (GPU). Our GPU implementation detected a surgical instrument in 31 ms, sufficient for real-time tracking at the 26 volumes per second rate of the ultrasound machine. A water tank experiment found instrument tip position errors of less than 0.2 mm, and an *in vivo* study tracked an instrument inside a beating porcine heart. The tracking results showed good correspondence to the actual movements of the instrument.

1 Introduction

Real-time three-dimensional ultrasound (3DUS) is a viable tool for guiding surgical procedures [1]. This visualization technique may enable a range of new minimally invasive procedures in cardiac surgery. For example, beating heart intracardiac surgery is now possible with the use of 3DUS and minimally invasive instruments [2][3]: ultrasound permits visualization through the opaque blood pool in the heart, and the advent of real-time 3DUS overcomes many of the difficulties with 3D spatial perception in conventional 2D ultrasound [1]. These procedures eliminate the need for a cardiopulminary bypass and its well documented adverse effects, including delay of neural development in children, mechanical damage from inserting tubing into the major vessels, increased stroke risk, and significant decline in acute and chronic cognitive performance [4][5][6].

Initial animal trials highlighted several obstacles to clinical implementation of ultrasound-guided intracardiac surgery [2][3]. One such limitation is instrument perception, due to the distorted appearance of stiff materials under 3DUS, including high noise levels, shadowing, and a variety of artifacts. To address this issue, researchers have developed techniques to detect instruments in ultrasound.

By detecting instruments as they move within the ultrasound image it is possible to highlight the position of the instrument for the surgeons. Eventually, this will allow surgeons to more accurately control the instruments as they perform a surgical task. For example, Vitrani *et al.* [7][8] tracked the fingers of a endoscopic grasper with 2D ultrasound. In addition, there have been numerous reports of tracking surgical needles with ultrasound [9]. These techniques, however, use 2D ultrasound or track instruments in homogeneous static tissue, which limits the applicability to the heterogeneous dynamic environment found in intracardiac procedures. Stoll *et al.* showed that instruments could be tracked in 3DUS using passive markers[10]. This implementation employed singular value decomposition for instrument shaft detection that was unable to distinguish instruments from tissue or other objects. It was also incapable of tracking instruments faster than 1.5Hz and therefore unsuitable for beating heart procedures.

In this work we present a technique capable of detecting instruments used in minimally invasive procedures. We build upon previous work by combining two methods: Radon transform-based instrument shaft detection in 3DUS [11] and passive markers for instrument tip localization [12]. These two methods are complimentary, and we describe a hybrid approach for complete 6 degree of freedom instrument tracking. In addition, we demonstrate that this hybrid technique is well-suited for implementation on powerful personal computer graphics processor units (GPUs). By using a GPU based approach, the complete system is capable of real-time tracking at the rate of the 26 volumes per second produced by the 3DUS machine. The tracking method is validated in water tank and *in vivo* experiments.

2 Methods and Materials

To attain real-time tracking of instruments within an 3DUS image, we utilized techniques that were especially amenable to high performance implementations. This consideration is especially important due to the high data rates of the real-time 3DUS, where volumes (204x48x148 voxels) are produced at a rate of 25-28 Hz. This high data rate requires that real-time algorithms must handle 40 MB of data every second. For this challenge, we build upon work presented by Novotny *et al.* [11], that introduces a high performance instrument shaft detection algorithm. We also incorporate passive markers similar to those presented in [12], but pay careful attention to marker design for increased performance.

2.1 Instrument Tracking

The first step is to detect the axis of the instrument. Generally, minimally invasive instruments such as those used in intracardiac procedures are fundamentally cylindrical in shape (Fig. 1). Graspers, scissors, needle drivers, and clip deployment devices are all attached to a long cylindrical tube. A modified form of the Radon transform has been shown to be capable of identifying these long straight

Fig. 1. *In vivo* 3D ultrasound image of a porcine heart with a 5 mm instrument inserted into the right atrium.

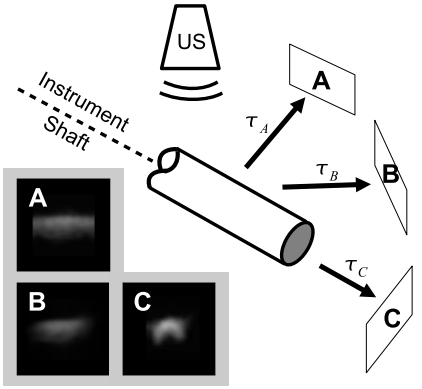

Fig. 2. Example of the modified Radon transform. Each image (A-C) is a projection of the ultrasound image along the direction (τ_A-τ_C).

cylinders (Fig. 2), a feature that is not found in cardiac ultrasound images [11]. The algorithm identifies maximums of the the equation:

$$\check{g}\left(\theta,\phi,u,v\right)=\int g\left(s\tau\left(\theta,\phi\right)+u\alpha\left(\theta,\phi\right)+v\beta\left(\theta,\phi\right)\right)ds \tag{1}$$

where $\check{g}$ is referred to as the modified Radon space of the ultrasound volume, g. Each point in $\check{g}$ corresponds to the integral along a three dimensional line defined by the four parameters θ, ϕ, u and v. The angular parameters, θ and ϕ, define an orthonormal basis composed of α, β, and τ that are defined as

$$\tau=\begin{pmatrix}cos\theta cos\phi\\ sin\theta cos\phi\\ sin\phi\end{pmatrix},\ \alpha=\begin{pmatrix}-sin\theta\\ cos\theta\\ 0\end{pmatrix},\ \beta=\begin{pmatrix}-cos\theta sin\phi\\ -sin\theta sin\phi\\ cos\theta\end{pmatrix}. \tag{2}$$

Two positional parameters, u and v, are also used to fully define a 3D line (Fig. 3). Identifying lines in a 3D volume now becomes a problem of finding local maximums of $\check{g}$. By finding the maximum value of $\check{g}$, the axis of the instrument in 3D space is implicitly defined by the parameters (θ,ϕ,u,v).

This algorithm is especially well suited for implementation on parallel architectures such as modern graphics processing units. In its original implementation it detected instruments in an ultrasound volume in 0.6 s [11]. To improve upon this previous implementation, we both refined the search algorithm that identifies maximums of Eqn. 1 and also used the information from previous volumes to seed the tracking of the current volume.

To this end, we start by calculating Eqn. 1 for evenly spaced points throughout the volume space g. Spatially, the volume is sampled at 5 voxel increments in x, y, and z. For angles θ and ϕ, Eqn. 1 is sampled in 10 degree increments. Due

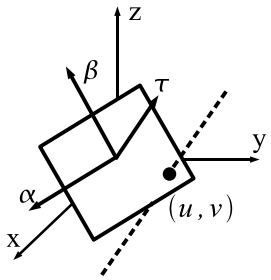

Fig. 3. Schematic of the modified Radon transform in 3D. The transform integrates along a line (shown as dashed), defined by α, β, and τ.

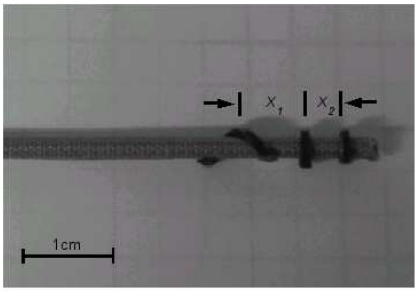

Fig. 4. Picture of an instrument with passive markers. The instrument tip and roll angle is calculated using the distances x_1 and x_2.

to symmetry, the angles are only sampled from 0 to 180 degrees. This search constitutes the initialization of the instrument tracking, as the entire volume is searched for the instrument. For 148x48x208 voxel volumes, this results in 408,000 iterations of Eqn. 1.

For subsequent frames, the tracking algorithm confines its search space to an area centered on the location found in the previous frame. Since the ultrasound volumes are updated at 25-28 Hz, this search space can be fairly small. In our trials, we empirically found that limiting the search space to ± 5 voxels spatially in the x, y, and z directions and ± 10 degrees around the angles θ and ϕ found in the previous frame was sufficient to capture typical surgical movements.

To enable real-time tracking, the instrument axis tracking algorithm is calculated on the GPU where the 3DUS volume is stored in texture memory. Each calculation of Eqn. 1 is performed by a pixel shader on the GPU. These pixel shaders take advantage of high performance volume interpolation and vector manipulation built into the GPU. In addition, the GPU used in the implementation (7800GT, nVidia Corp, Santa Clara, CA) has 16 pipelines that calculate Eqn. 1 simultaneously for 16 different positions in the $\check{g}$ space. Once the $\check{g}$ space has been sufficiently sampled, the maximum identifies the position of the instrument axis.

2.2 Passive Markers

Once the axis of the instruments is found, it is necessary to detect the final two degrees of freedom of the instrument (tip position and roll angle) to fully define its position and orientation. To this end, we build on work first introduced by Stoll *et al.* [12]. Here we use a new marker design, shown in Fig. 4. To produce distinct elements, 800 μm polyurethane foam was wrapped around the instrument shaft as shown in Fig. 4. Uncoated metals such as the stainless steel used for surgical instruments are highly reflective in ultrasound. To ensure that the instrument is visible in ultrasound, a more diffusive interaction with the

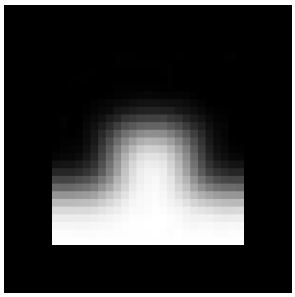

Fig. 5. Passive marker template.

Fig. 6. 3D ultrasound image of a surgical instrument in a water tank with white dots indicating tracked passive markers.

ultrasound pulse is desired. As a result, an 80 μm fiberglass embedded PTFE coating was applied to the instrument in order to improve the appearance.

Finding the markers begins with the image volume already loaded into texture memory from the Radon transform algorithm, then the built-in tri-linear interpolation is used to quickly render a slice through the instrument axis, orientated so that the instrument axis is horizontal. To identify the position of the bumps, a template matching algorithm is used on the ultrasound slice. The algorithm uses the sum of the absolute differences between a candidate region of the slice and a template, shown in Fig. 5.

The positions of the three best matches found in the slice are used to determine the tip position of the instrument and the roll angle (Fig. 6). The tip position is found with a known offset of 3 mm between the two closest markers and the instrument tip. To find the roll angle, the ratio of the distances x_1 and x_2 is used (Fig. 4). Since the third marker is wrapped in a helical pattern around the instrument shaft, the roll angle is a linear function of this ratio.

The configuration of these markers was designed to minimize the computational complexity for real-time implementation. Although there are more compact and higher-resolution marker designs [12], they result in time consuming calculations. In this implementation, the calculations are linear and negligibly add to the computational requirements of the algorithm.

2.3 Experimental Setup

The system uses a Pentium 4 3 GHz personal computer with 1 GB of RAM. The ultrasound machine (SONOS 7500, Philips Medical, Andover, MA) streamed image data over a 1 Gb LAN to a personal computer using TCP/IP. A program written in C++ retrieved the ultrasound volumes and loaded them onto the GPU (7800GT, nVidia Corp, Santa Clara, CA) through a PCI-express bus.

To prove the effectiveness of the complete instrument tracking algorithm, we performed two validation experiments. The first was a water tank study and measured the accuracy of the full six degree of freedom instrument tracking.

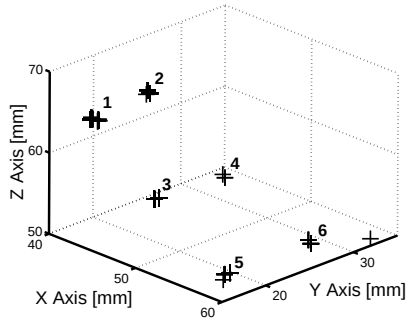

Fig. 7. Plot of the tip location for an instrument in 1 cm spaced positions in a water tank.

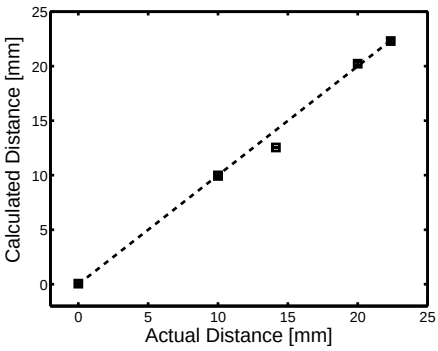

Fig. 8. Distance from position 1 calculated by the tracking algorithm.

Six positions on a acetyl block were marked in a 1 cm rectangular pattern. The ultrasound probe and 6 marked positions were held statically, while the instrument was moved from position to position. At each of the 6 positions the instrument was imaged for 5 s. The tip position calculated by the tracking algorithm was logged to a data file for analysis.

Second, *in vivo* validation was performed by tracking an instrument within a beating porcine heart. Electromagnetic tracking (miniBIRD 800, Ascension Technology, Burlington, VT) was used to simultaneously track the instrument tip position. The instruments were imaged inside a porcine heart during an open chest beating heart procedure. The instruments were inserted through ports in the right atrial wall and secured by purse-string sutures. The ultrasound probe was positioned epicardially on the right atrium to give a view of the right and left atrium. The surgeon was instructed to move the instrument toward the atrial septum. During this movement, the instrument tip position calculated by the algorithm and the tip position measured by the electromagnetic trackers was recorded to a data file.

3 Results

The algorithm was shown to be effective at real-time tracking surgical instruments in both the water tank and *in vivo* experiments. In the tank experiment, the tracking algorithm accurately measured the relative distances traveled by the instrument tip as it moved to 6 positions 1 cm apart on an acetyl block. Fig. 7 shows the tip positions as reported by the algorithm. The estimated distance of points 2-5 from point 1 is shown in Fig. 8; these distances correspond to the actual separation of the six points marked on the block. The algorithm found distances to points 2 and 3 with a mean error of 0.0 mm and with standard deviation of 0.1 mm. The distance to point 4 showed the largest mean error

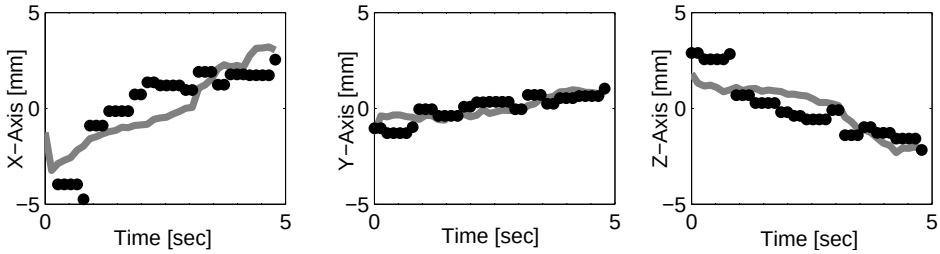

Fig. 9. *In vivo* x, y, and z position of the instrument tip as reported by an electromagnetic tracker (solid line) and the tracking algorithm (dots).

of 1.6 mm±0.01 mm and points 5 and 6 had mean errors of 0.2±0.1 mm and 0.1±0.1 mm, respectively.

Fig. 9 shows the results of the *in vivo* trials. The figure plots the x, y, and z trajectories of the instrument tip versus time. Both the instrument tip position reported by the instrument tracking algorithm and the electromagnetic trackers is shown. The tracking method correctly tracked the instrument tip as the surgeon moved it for 5 s. The mean difference between the tip position reported by the electromagnetic tracker and tracking algorithm was 1.4 mm, 0.4 mm, and 0.9 mm in x, y, and z directions.

In our experimental setup, the instrument tracking technique required 1.7 s to initially detect the instrument in the entire ultrasound volume. For subsequent tracking, the algorithm required 32 ms per volume. This speed is well within the 38 ms required for the algorithm to keep pace with the 26 volumes per second generated by the ultrasound machine.

4 Discussion

These results show that real-time tracking of surgical instruments is possible with 3DUS. The method successfully integrates Radon transform-based instrument axis tracking and passive marker-based tip and roll tracking to determine the full 6 degrees of freedom of the instrument. In addition, by harnessing the computational power of the GPU and using a fast search schema, the tracking system kept pace with the 25-28 volumes per second produced by the 3DUS machine. To the authors knowledge, this is the first demonstration of real-time tracking of surgical instruments *in vivo* with 3DUS.

The tank experiments highlighted the accuracy of the technique, within 0.2 mm for most cases. However, as seen in one of the measurements (Fig. 8), the marker detection algorithm incorrectly identifies the position of the passive markers. As a result, the tip position is incorrectly calculated along the shaft axis. Further research is underway to improve upon the marker template matching procedure, and to introduce predictive filters to improve accuracy.

In vivo trials provided verification of the effectiveness of the algorithm when instruments are surrounded by blood and highly inhomogeneous and rapidly

moving tissue within the beating heart. The electromagnetic tracking used for verification is by no means a "gold standard", as it is highly susceptible to electromagnetic interference that is found in a modern operating room. It did provide a corroborative data set that showed the tracking technique presented here is in fact tracking the surgical instrument. A more rigorous study into how accurately the method performs *in vivo* is left for future work.

By developing a real-time instrument tracking technique, it is now possible to introduce a range of improvements to aid in our target procedures, intracardiac surgery. Real-time tracking can now be used for instrument overlays and navigational aids to help the surgeon deal with the distorted appearance of tissue and instruments in 3DUS images. In addition, tracking of instruments opens a wide range of possibilities for implementing robot control under 3DUS guidance.

5 Acknowledgments

This work is supported by the National Institutes of Health under grant NIH R01 HL073647-01.

References

1. Cannon, J.W., et al.: Real time 3-dimensional ultrasound for guiding surgical tasks. Computer Assisted Surgery **8**(2) (2003) 82–90
2. Suematsu, Y., et al.: Three-dimensional echocardiography-guided beating-heart surgery without cardiopulmonary bypass: a feasibility study. J Thorac Cardiovasc Surg. **128** (2004) 579–587
3. Suematsu, Y., et al.: Three-dimensional echo-guided beating heart surgery without cardiopulmonary bypass: atrial septal defect closure in a swine model. J Thorac Cardiovasc Surg. **130**(5) (2005) 1348–57
4. Murkin, J.M., et al.: Beating heart surgery: Why expect less central nervous system morbidity? Annals of Thoracic Surgery **68** (1999) 1498–1501
5. Zeitlhofer, J., et al.: Central nervous system function after cardiopulmonary bypass. European Heart Journal **14**(7) (1993) 885–890
6. Bellinger, D., et al.: Developmental and neurological status of children at 4 years of age after heart surgery with hypothermic circulatory arrest or low-flow cardiopulmonary bypass. Circulation **100** (1999) 526–532
7. Vitrani, M., Morel, G., Ortmaier, T.: Automatic guidance of a surgical instrument with ultrasound based visual servoing. Proc. IEEE ICRA (2005) 510–515
8. Ortmaier, T., et al.: Robust real-time instrument tracking in ultrasound images for visual servoing. Proc. IEEE ICRA (2005) 2167–72
9. Draper, K., et al.: An algorithm for automatic needle localization in ultrasound-guided breast biopsies. Medical Physics **27** (2000) 1971–9
10. Stoll, J., Novotny, P., Dupont, P., Howe, R.: Real-time 3d ultrasound-based servoing of a surgical instrument. Proc. IEEE ICRA (2006)
11. Novotny, P., Zickler, T., Howe, R.: Radon transform based instrument shaft detection in three-dimensional ultrasound. submitted (biorobotics.harvard.edu/pubs/NovotnyTMI.pdf) (2006)
12. Stoll, J., Dupont, P.: Passive markers for ultrasound tracking of surgical instruments. MICCAI (2005)